Supporting Information

Shape Matters: Enhanced Osmotic Energy Harvesting in Bullet-shaped Nanochannels

Gregorio Laucirica,[1] Alberto G. Albesa,[1] María Eugenia Toimil-Molares,[2]
Christina Trautmann,[2,3] Waldemar A. Marmisollé,[1,*] and Omar Azzaroni[1,*]

[1]Instituto de Investigaciones Fisicoquímicas Teóricas y Aplicadas (INIFTA) – Departamento de Química – Facultad de Ciencias Exactas – Universidad Nacional de La Plata (UNLP) – CONICET, Diagonal 113 and 64 –La Plata (1900) Argentina.

[2]GSI Helmholtzzentrum für Schwerionenforschung, 64291 Darmstadt, Germany

[3]Technische Universität Darmstadt, Materialwissenschaft, 64287 Darmstadt, Germany

e-mail: azzaroni@inifta.unlp.edu.ar

e-mail: wmarmi@inifta.unlp.edu.ar

Bullet-shaped geometry

The bullet-shaped geometry was confirmed by *Scanning Electron Microscopy* (SEM) (**Figure S1**). For this purpose, multi-pore membranes (10^9 pores/cm^2) were exposed to a surfactant-assisted etching as explained in the main text. After etching, the samples were irradiated with UV light and then were exposed to liquid nitrogen with the aim of breaking down the foil. Finally the membrane was mounted at 90° in order to obtain the cross-section images. In all cases the parabolic profile in the region around the tip can be noted.

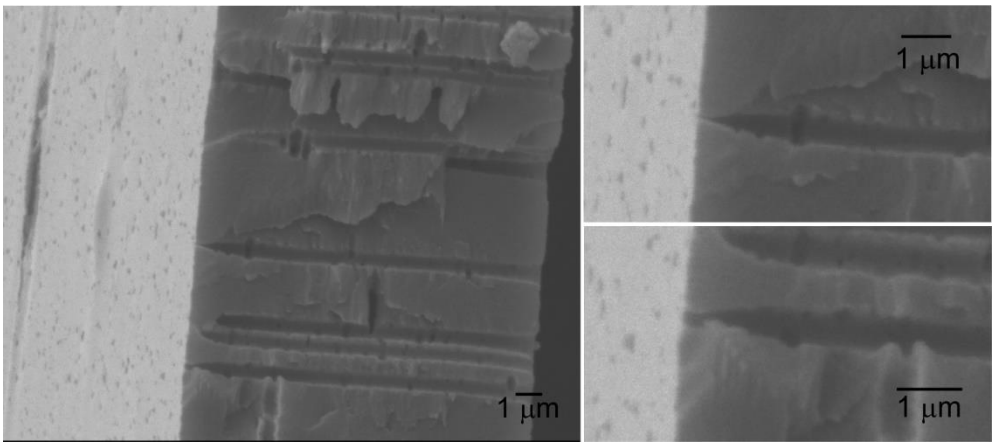

Figure S1. *SEM images of cross-sections of multi-pore membranes exposed to a surfactant-assisted etching.*

The profile of bullet-shaped nanochannels along the length x can be computed by

$$D(x) = D - (D - d_{tip})\exp(-x/h) \qquad \textbf{(eq. S1)}$$

with D being the base diameter; d_{tip} the tip diameter and h a parameter that accounts for the curvature of the bullet-shaped opening (see **Figure S2**).

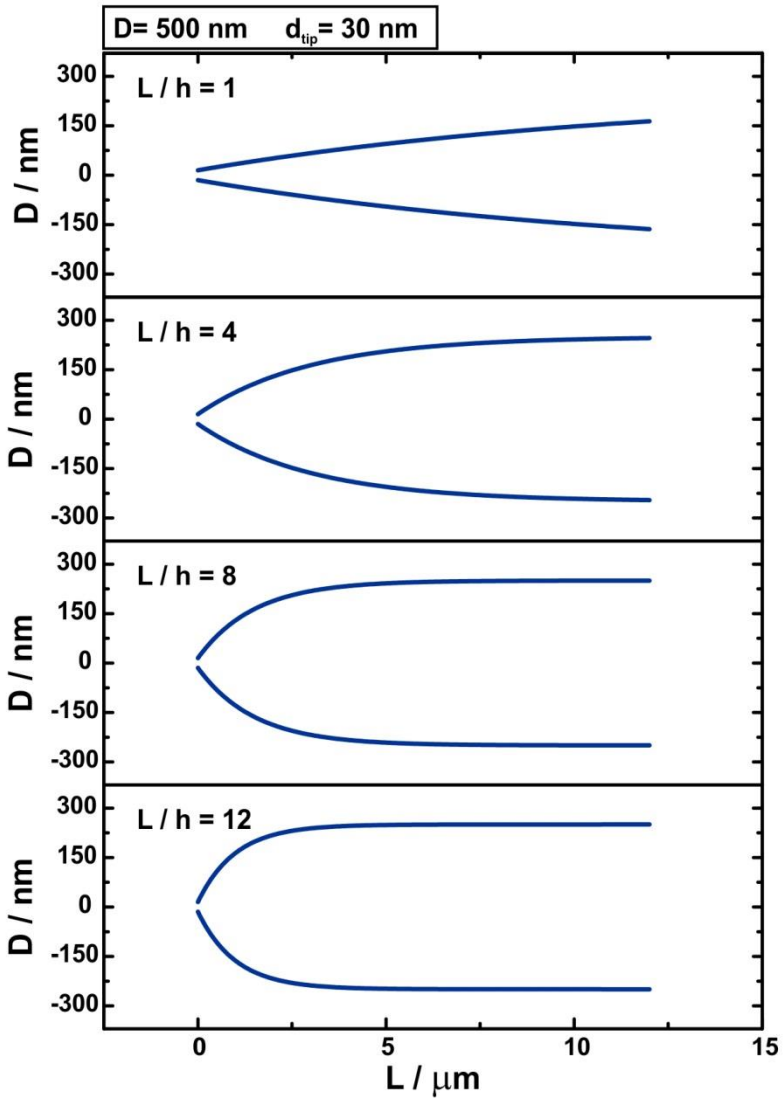

Figure S2. *Asymmetric bullet-shaped nanochannel profiles for different L/h values. Tip and base diameters were fixed at 30 nm and 500 nm, respectively.*

Bullet-shape characterization by Poisson–Nernst–Planck simulations

The Poisson–Nernst–Planck (PNP) model allows the quantitative description of ion transport across the channel by solving the Poisson, Nernst-Planck and continuity equations. A seminal article by Cervera *et. al.* demonstrated the validity of this model for the study ion transport in track-etched nanochannels [1,2]. In this work, the PNP formalism was used to determine bullet-shaped channel geometrical parameters from experimental i-V curves (experimental details about the model are available in Ref [3,4]). For this aim, the surface charge density was fixed at -1.5 e/nm^2 whereas the geometrical parameters were fitted. **Figures S3 (A)** and **(B)** shows a good correlation between the experimental curves and those obtained via PNP simulation. The results are summarized in the main text (**Table 1**).

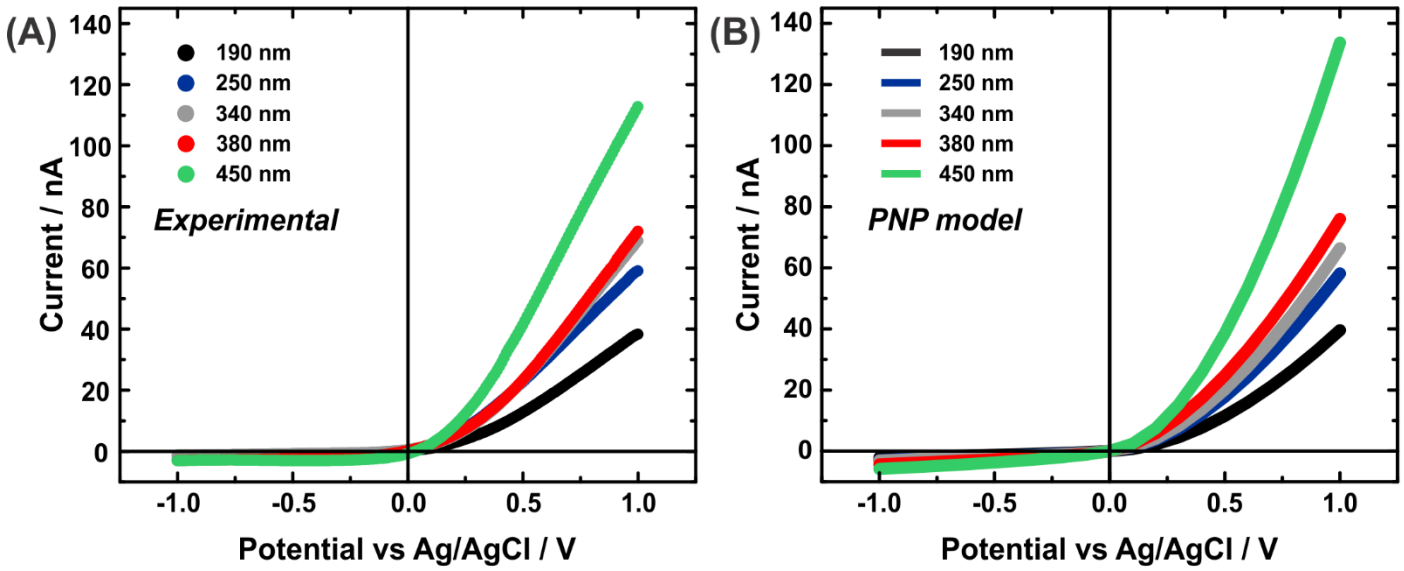

Figure S3. *(A) Experimental and (B) theoretical i-V curves recorded at 0.1 M KCl and pH=10. The values given in the graphs denote D_{eff}, the effective channel diameter as defined by eq.3.*

Effective diameter and bullet-shaped parameters

At high enough ionic strength, the resistance R can be computed from the conductivity k of the solution inside the channels neglecting the surface charge effects. The resistance of a disc of thickness *dx* and diameter *D(x)* can be computed as

$$dR = \frac{dx}{\kappa A} = \frac{4dx}{\kappa\pi D^2(x)} = \frac{4dx}{\kappa\pi\left[D-(D-d_{tip})\exp(-x/h)\right]^2} \qquad \textbf{(eq. S2)}$$

where A is the cross-section area. The total resistance can be determined by integration along the nanochannel length as

$$R = \frac{4}{\kappa\pi}\int_0^L \frac{dx}{\left[D-(D-d_{tip})\exp(-x/h)\right]^2} \qquad \textbf{(eq. S3)}$$

Using the following indefinite integral,

$$\int \frac{dx}{(p+qe^{ax})^2} = \frac{x}{p^2} + \frac{1}{ap(p+qe^{ax})} - \frac{1}{ap^2}\ln(p+qe^{ax}), \qquad \textbf{(eq. S4)}$$

The integration along the entire channel yields a total resistance of

$$R = \frac{1}{\kappa\pi}\left[\frac{x}{D^2} - \frac{h}{D(D-(D-d_{tip})e^{-x/h})} + \frac{h}{D^2}\ln(D-(D-d_{tip})e^{-x/h})\right]_0^L \qquad \textbf{(eq. S5)}$$

which results in

$$R = \frac{4L}{\kappa\pi D^2}\left[1 + \frac{h}{L}\left\{\frac{1}{d'} - \frac{1}{(1-(1-d')e^{-L/h})} + \ln\frac{(1-(1-d')e^{-L/h})}{d'}\right\}\right];\ \ d' = d_{tip}\,/\,D \qquad \textbf{(eq. S6)}$$

where the first factor corresponds to the resistance of a cylindrical channel of diameter D (case d_{tip}=D).

As commented in the article, sometimes it is useful to define an effective diameter as

$$R = \frac{4L}{\kappa\pi D_{eff}{}^2} \qquad \textbf{(eq. S7)}$$

Comparing eq. S7 and S6 gives

$$\frac{1}{D_{eff}{}^2} = \frac{1}{D^2}\left[1 + \frac{h}{L}\left\{\frac{1}{d'} - \frac{1}{(1-(1-d')e^{-L/h})} + \ln\frac{(1-(1-d')e^{-L/h})}{d'}\right\}\right] \qquad \textbf{(eq. S8)}$$

A limit expression can be derived for the case d'=d_{tip}/D<<1 and L/h >1,

$$D_{eff} \approx \left[d_{tip} D \frac{L}{h}\right]^{1/2} \qquad \textbf{(eq. S9)}$$

pH-effect on the energy conversion performance

The analysis of the energy conversion performance was realized through the *i-V* curves performed under a concentration gradient of the electrolyte. The base side of the channel was exposed to a high concentration (C_H) of KCl (1000 mM) and the tip side was exposed to a low concentration (C_L) of KCl between 1 mM and 100 mM. All measurements were carried out at pH=10, where a large amount of the carboxylates is expected to be dissociated. This point is supported by the variation of the rectification factor with pH (**Figure S4**). In absence of a change of channel size, wettability and electrolyte concentration, the increase of the rectification factor with pH is ascribed to an increase of surface charges. Moreover, for pH>10, the OH^- concentration would lead to a decrease in the rectification factor because of the high diffusion coefficient of OH^- in comparison with Cl^-.

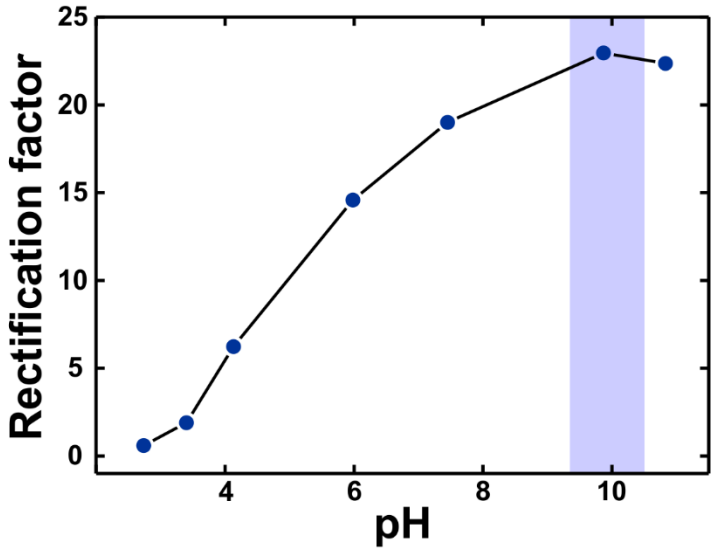

Figure S4. *Rectification factor for different pH values in a bullet-shaped nanochannel. The measurements were performed in KCl 0.1 M. Here the rectification factor is defined as I(1V)/I(-1V).*

For ion-selective membranes, the surface charge directly affects the performance of the system. For this reason, it is expected that the pH value has a significant influence on the power obtained. In order to maximize the power, the performance at pH ~5.6-6 (pure mQ water) and pH=10 was evaluated applying a salinity gradient of 1000-fold (i.e. C_L=1 mM KCl and C_H= 1000 mM KCl) (**Figure S5**). As expected, the basic pH values improve the energy harvested.

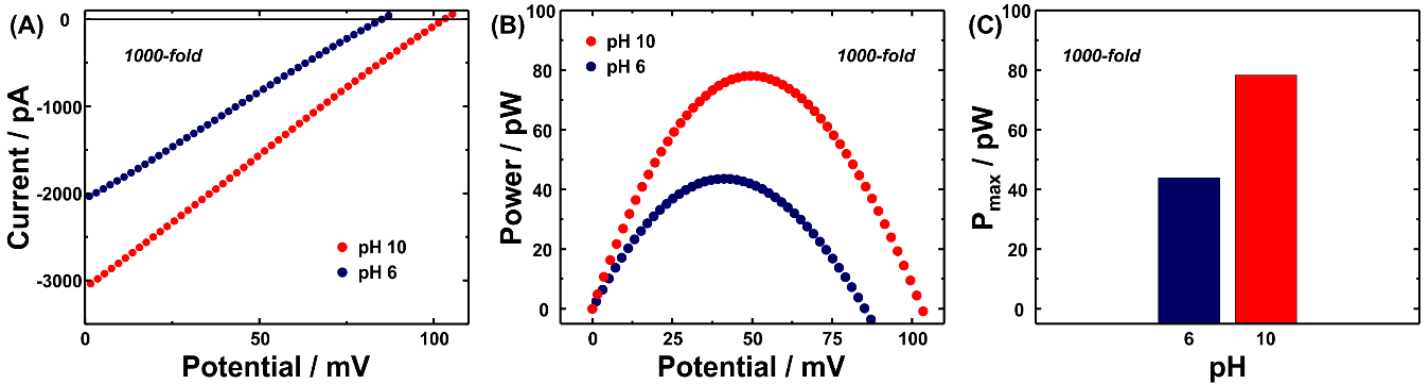

Figure S5. *Measurements for a nanochannel at pH=6 and pH=10 for a KCl electrolyte gradient of 1000-fold (C_L=1 mM KCl and C_H= 1000 mM KCl) (A) i-V curves (B) Power-Voltage curves (C) Maximum output power; at pH=10 P_{max} is enhanced by approximately 57%.*

The salinity gradient imposed is a relevant parameter in the performance of the device. In the range studied, all devices presented the best performance for the maximum value of $\log(C_H/C_L)$. This fact is explained because both the zero-volt current $|i_o|$ and the reversal potential V_{rev} grow with increasing $\log(C_H/C_L)$ (**Figure S6**).

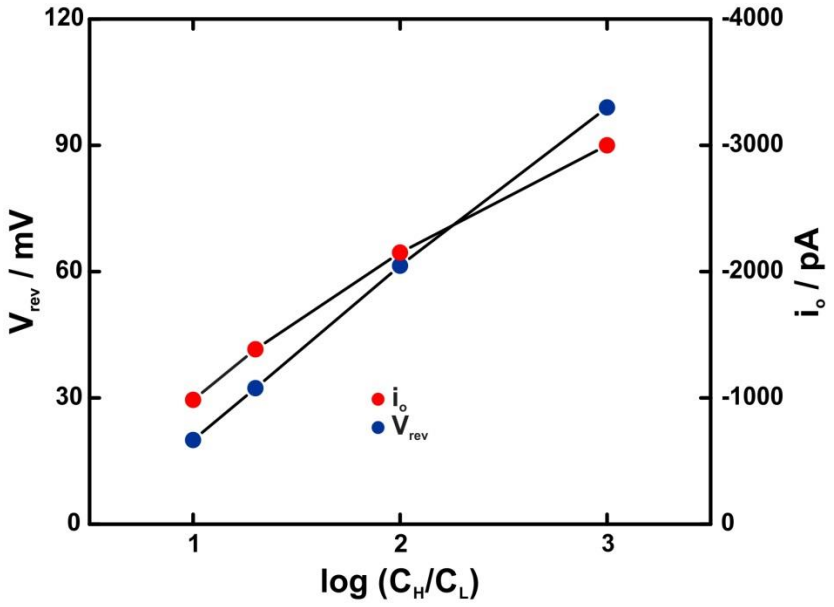

Figure S6. *Zero-volt current $|i_o|$ and reversal potential V_{rev} as a function of the concentration gradient C_H/C_L imposed. In both cases, the increase of the gradient produced an increment in the absolute value.*

As in the case of symmetric conditions (C_H=C_L), *i-V* in the presence of a concentration gradient follows a non-ohmic behavior (**Figure S7 (A)** and **(B)**). The direction of the rectification is inverted and the absolute value decreases (**Figure S7 (C)**). This anomalous trend was previously analyzed by Cao *et. al.*[5]. The iontronic output of a nanochannel submitted to a concentration gradient has two contributions (**Figure S6(D)**). The

concentration of ions in the channel, and therefore the current, is not only given due to the application of electric potential but also by the diffusion of ions from high to low KCl concentration. For symmetric KCl conditions, the iontronic output exhibited a low conductance region for negative potentials due to the exclusion of co-ions. However, when the measurement was performed in asymmetric KCl conditions, the ion diffusion produced an increment in ion concentration in the channel which increases the current. For lower gradients applied, ion diffusion contributes less explaining the diminution of rectification inversion (**Figure S6 (C)**).

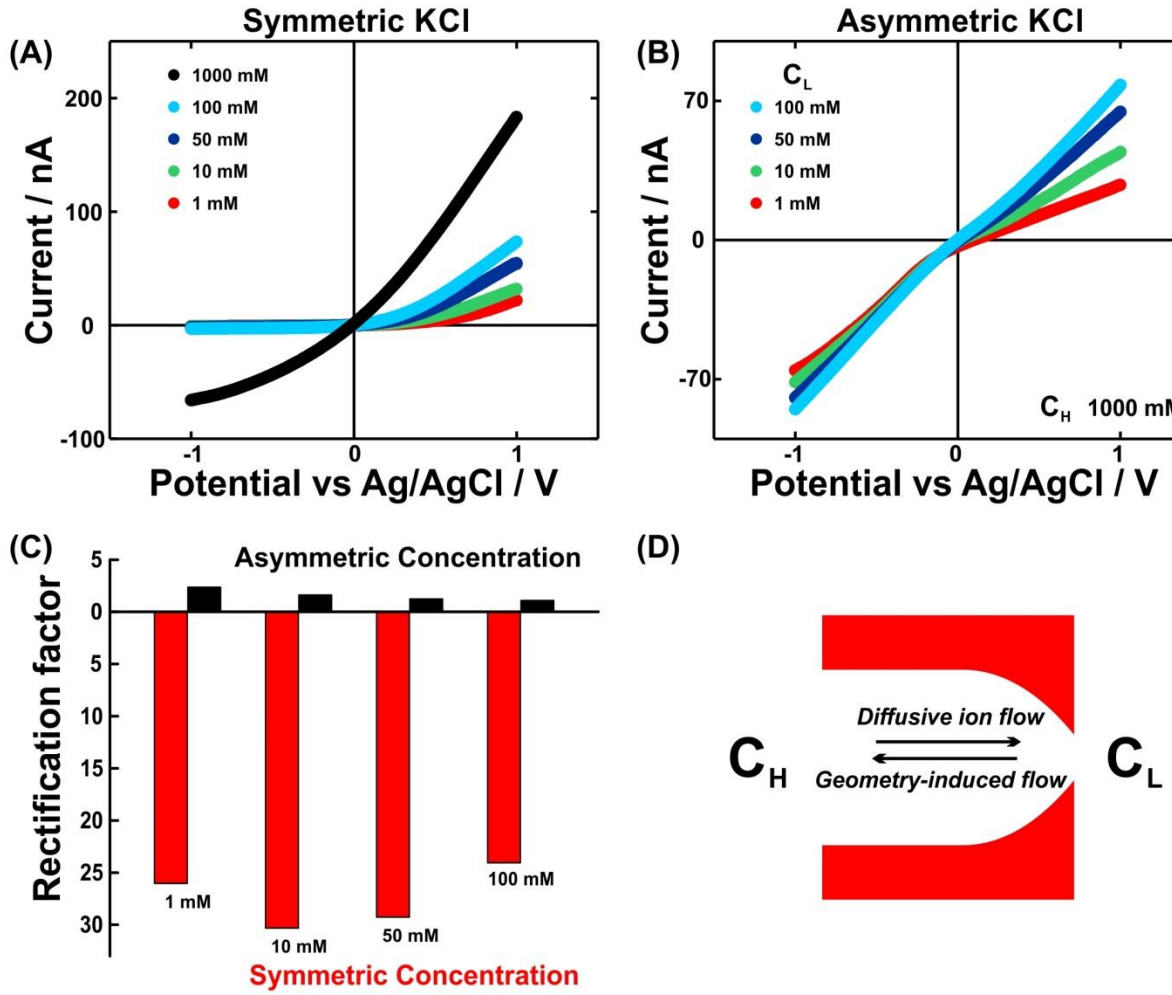

Figure S7. *i-V curves under (A) symmetric and (B) asymmetric KCl concentrations at pH=10 (C_H was fixed to 1000 mM; C_L values are in the plot). (C) Rectification factor for the i-V curves: symmetric (red) and asymmetric (black) conditions. (D) General scheme of the processes that contribute to the iontronic output under asymmetric electrolyte conditions.*

The asymmetric profile of bullet-shaped nanochannels putatively leads to the increment of maximum power in comparison with other channel geometries. This fact can be explained by the lower channel resistance due to the high base diameter and, at the same time, the high ionic selectivity achieved by the tip region. On the other side, there is no direct correlation between the channel effective size and maximum power, as observed in **Figure S8.**

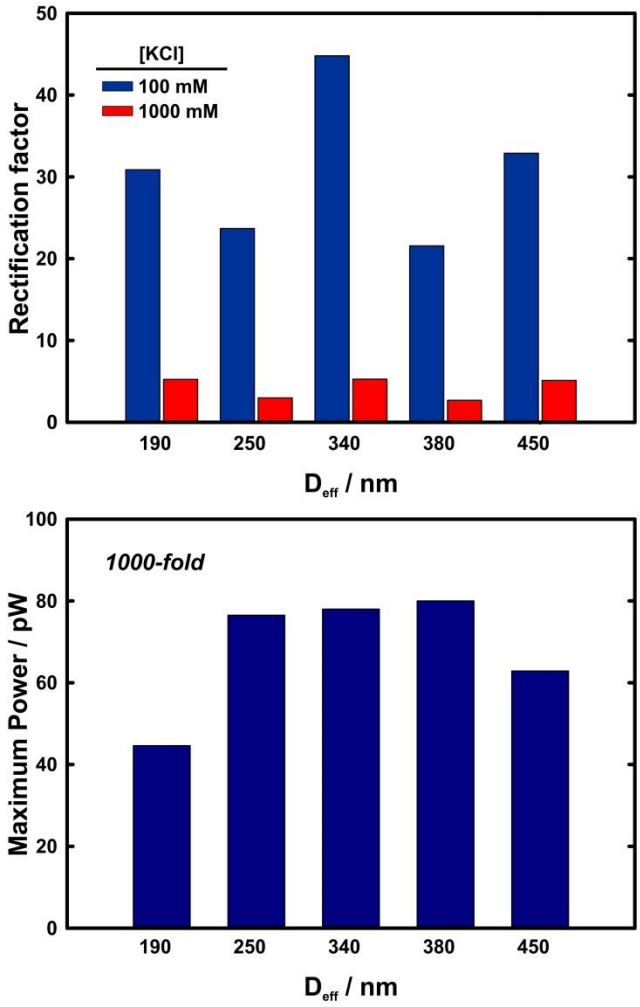

Figure S8. *(A) Rectification factor of nanochannels with different D_{eff} in symmetric conditions. (B) Maximum Power obtained for the different nanochannels applying a 1000-fold gradient.*

In line with the cation transference number, in most cases, the efficiency η could be improved by maximizing the gradient applied (**Figure S9**) because the electrolyte concentration drops on the tip side. This fact causes an enlargement of EDL and, consequently, an increment in the selectivity that has an impact on the efficiency. As expected from the trend of t_+, in some cases the maximization of C_H/C_L produced a small drop on the efficiency. It is important to clarify that the improvement in the efficiency with the increasing of C_H/C_L is because C_H was fixed and C_L was varied. The transport number does not just depend on the quotient C_H/C_L but also on the specific value of C_H, C_L, the orientation of the channel, the salt, among others [6–8].

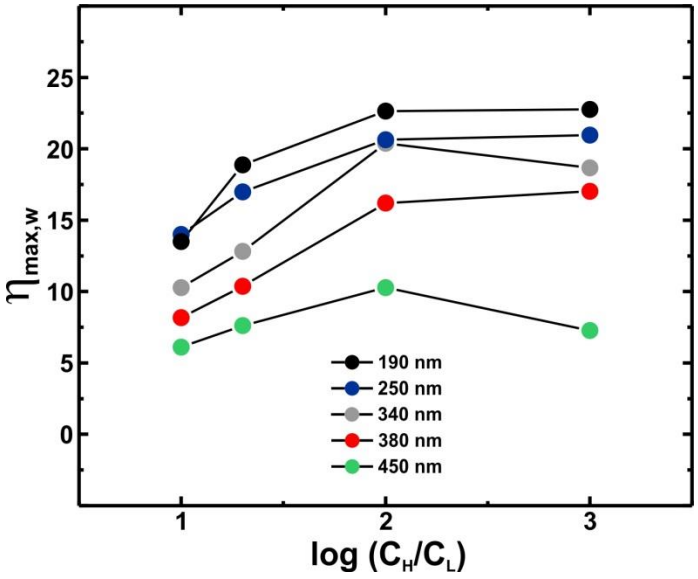

Figure S9. *Efficiency* η *and gradient applied for the different channels. All measurements were carried out at pH=10.*

References

[1] J. Cervera, B. Schiedt, R. Neumann, S. Mafá, P. Ramírez, Ionic conduction, rectification, and selectivity in single conical nanopores, J. Chem. Phys. 124 (2006).

[2] J. Wang, M. Zhang, J. Zhai, L. Jiang, Theoretical simulation of the ion current rectification (ICR) in nano-pores based on the Poisson-Nernst-Planck (PNP) model, Phys. Chem. Chem. Phys. 16 (2014) 23–32.

[3] G. Pérez-Mitta, A.G. Albesa, W. Knoll, C. Trautmann, M.E. Toimil-Molares, O. Azzaroni, Host-guest supramolecular chemistry in solid-state nanopores: potassium-driven modulation of ionic transport in nanofluidic diodes., Nanoscale. 7 (2015) 15594–8.

[4] G. Pérez-Mitta, A.G. Albesa, M.E. Toimil Molares, C. Trautmann, O. Azzaroni, The Influence of Divalent Anions on the Rectification Properties of Nanofluidic Diodes: Insights from Experiments and Theoretical Simulations, ChemPhysChem. (2016) 2718–2725.

[5] L. Cao, W. Guo, Y. Wang, L. Jiang, Concentration-gradient-dependent ion current rectification in charged conical nanopores, Langmuir. 28 (2012) 2194–2199.

[6] J. Cervera, A. Alcaraz, B. Schiedt, R. Neumann, P. Ramírez, Asymmetric selectivity of synthetic conical nanopores probed by reversal potential measurements, J. Phys. Chem. C. 111 (2007) 12265–12273.

[7] P. Ramirez, J. Cervera, V. Gomez, M. Ali, S. Nasir, W. Ensinger, et al., Membrane potential of single asymmetric nanopores : Divalent cations and salt mixtures, J. Memb. Sci. 573 (2019) 579–587.

[8] L. Cao, W. Guo, W. Ma, L. Wang, F. Xia, S. Wang, et al., Towards understanding the nanofluidic reverse electrodialysis system: Well matched charge selectivity and ionic composition, Energy Environ. Sci. 4 (2011) 2259–2266.